Acta Cryst A FOUNDATIONS ADVANCES

ISSN 2053-2733

Derived crystal structure of martensitic materials by solid–solid phase transformation

Mostafa Karami,[a] Nobumichi Tamura,[b] Yong Yang[c] and Xian Chen[a]*

[a]Mechanical and Aerospace Engineering, Hong Kong University of Science and Technology, Hong Kong, [b]Advanced Light Source, Lawrence Berkeley National Laboratory, California, USA, and [c]Mechanical Engineering, City University of Hong Kong, Hong Kong. *Correspondence e-mail: xianchen@ust.hk

Received 26 September 2019
Accepted 4 May 2020

Edited by S. J. L. Billinge, Columbia University, USA

Keywords: derived lattice; martensitic phase transformation; structure determination; synchrotron X-ray diffraction.

A mathematical description of crystal structure is proposed consisting of two parts: the underlying translational periodicity and the distinct atomic positions up to the symmetry operations in the unit cell, consistent with the *International Tables for Crystallography*. By the Cauchy–Born hypothesis, such a description can be integrated with the theory of continuum mechanics to calculate a derived crystal structure produced by solid–solid phase transformation. In addition, the expressions for the orientation relationship between the parent lattice and the derived lattice are generalized. The derived structure rationalizes the lattice parameters and the general equivalent atomic positions that assist the indexing process of X-ray diffraction analysis for low-symmetry martensitic materials undergoing phase transformation. The analysis is demonstrated in a CuAlMn shape memory alloy. From its austenite phase ($L2_1$ face-centered cubic structure), it is identified that the derived martensitic structure has orthorhombic symmetry *Pmmn* with the derived lattice parameters $a_d = 4.36491$, $b_d = 5.40865$ and $c_d = 4.2402$ Å, by which the complicated X-ray Laue diffraction pattern can be well indexed, and the orientation relationship can be verified.

1. Introduction

Martensitic materials show great potential in many emerging applications such as biomedical implants, nano/microactuators and solid-state caloric coolings because of their ability to recover a large macroscopic deformation (*i.e.* 5–10%) during the reversible structural transformation (Chang & Read, 1951; Tadaki, 1998; Miyazaki *et al.*, 1982). In real applications, these materials are required to run millions of transformation cycles, yet their functionality typically degrades quickly in the first couple of hundreds of cycles, even for the most successful commercial alloy Nitinol (Otsuka & Ren, 2005). Recent significant advances in developing ultra low fatigue martensitic materials (Song *et al.*, 2013; Chluba *et al.*, 2015) show that the design of phase-transforming materials can be guided through some kinematic compatibility principles called cofactor conditions (Chen *et al.*, 2013), *i.e.* the supercompatibility conditions for the existence of stressed-free microstructure during phase transformation. When the cofactor conditions are satisfied, the thermal hysteresis is minimized without compromising the amount of latent heat (Song *et al.*, 2013). Meanwhile the thermomechanical response does not degrade at all even upon tens of millions of mechanically induced transformation cycles (Chluba *et al.*, 2015). These discoveries underlie a theory-driven design strategy for phase-transforming materials, of which the most crucial step is to precisely determine the crystal structures of the transforming material as austenite

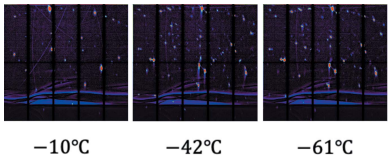

(high-symmetry structure in the high-temperature phase) and martensite (low-symmetry structure in the low-temperature phase). However, this step is non-trivial, and often quite tedious.

In principle, the structural parameters of a crystalline solid are determined by X-ray diffraction (XRD) experiments. One of the most common XRD measurements used for structural determination is Rietveld refinement of powder diffraction data obtained with either Cu $K\alpha$ or Mo $K\alpha$ radiation (Young, 1993). The testing specimen should be either in powder or bulk form with sufficient randomization of grain orientations illuminated by the monochromatic X-ray beam. However, the as-cast metallic specimen after proper heat treatment produced in a laboratory is mostly in bulk form with a coarse grain size. For example, the grain size of common Cu-based β alloys is about 200–500 µm (Bhattacharya *et al.*, 2003). The orientation randomness of the specimen from laboratory production is insufficient for the ordinary XRD powder method, especially for the low-symmetry structures. In most cases, the crystal structure of the developed material is unknown, which makes the Rietveld analysis impossible. On the other hand, the structure determination through single-crystal XRD requires isolated good-quality single crystals and is therefore hardly applicable to the bulk samples. The lack of structural knowledge for low-symmetry metallic materials greatly hinders the development of desirable properties. Therefore, it is very important to have a unified way for structural determination especially when the preliminary crystallographic information is limited.

The martensite phase forms from a high-temperature phase, austenite, through a solid–solid phase transformation, known as the martensitic transformation. This transformation can be reversible, as seen in shape memory alloys, if the point group of martensite is a subgroup of the point group of austenite, while it can be irreversible, as seen in steels, if the group–subgroup relationship breaks down (Bhattacharya *et al.*, 2004). In both cases, the martensite lattice can be considered as the deformed austenite lattice, which is characterized by the transformation strains based on specific orientation relationships. For example, the body-centered cubic α-Fe formed from the face-centered cubic γ-Fe is derived by the Bain correspondence that gives the Bain strains (Bain, 1924). Due to the lattice symmetry, there are various crystallographically equivalent ways to distort the austenite lattice to form different variants of martensite. For reversible martensitic transformations, the number of distinct martensite variants is characterized by the quotient of the order of the point group of the austenite lattice divided by the order of the point group of the martensite lattice. For reconstructive transformation such as precipitation, the precipitates can be treated as the deformed configuration from the matrix phase through a stretch tensor (Chen *et al.*, 2011). The formation of a semi-coherent interface between ellipsoid precipitates and the matrix depends on the weak compatibility conditions given by the stretch tensor and its crystallographically equivalent variants (Chen *et al.*, 2011). The nature of the martensitic transformation and the conditions of crystallographic compatibility between austenite and martensite can be used to propose a universal structural determination method for the martensite structure transformed from the austenite structure with cubic symmetry. The cubic structures, including simple cubic, face-centered cubic and body-centered cubic, have only one structural dimensional parameter, a_0, that can be accurately determined by ordinary XRD experiments. The martensite structure generated from austenite through certain lattice correspondence and distortions can be derived based on the Cauchy–Born rule for solid–solid phase transformation (Bhattacharya *et al.*, 2003; Ericksen, 2008; Weinan & Ming, 2007; Chen, Song *et al.*, 2016). Slight lattice parameter perturbation of the derived lattice is needed to generate the initial structural parameters for advanced structural characterization and analysis such as XRD, electron backscatter diffraction (EBSD) and so on.

In this paper, we provide the fundamental formulation for the derived lattice from a cubic structure based on the Cauchy–Born rule. We then use a synchrotron Laue X-ray microdiffraction experiment combined with energy scans to demonstrate our method for an unknown Cu-based β alloy. To bridge the discrepancy between the previous mathematical description of the lattice (Ball *et al.*, 1992; Pitteri, 1998) and the symmetry calculation of crystal structures by the *International Tables for Crystallography* (Hahn *et al.*, 1983), we propose a modified description for the crystal structure consisting of two parts: underlying translational periodicity and the fractional atomic positions in the unit cell consistent with the general equivalent positions used in the *International Tables for Crystallography*. By considering the parent and child phases as two discrete vector spaces mapped by a homogeneous linear transformation, the orientation relationship can be generalized and the associated vector/planar parallelisms can be defined.

2. Derived crystal structure from solid–solid phase transformation

2.1. Bravais lattice

Our theoretical calculations in this paper are adapted to both reversible martensitic (Ericksen, 1991) and reconstructive (Tolédano & Dmitriev, 1996) transformations in crystalline solids. The continuum mechanics theories as well as the non-linear crystallographic theory of martensite (Bhattacharya *et al.*, 2003) are used to underpin the framework of the derived structure from cubic austenite. The symmetry-breaking structural transformations are characterized by a set of stretch tensors, which are defined as the martensitic variants by Ball and James (Ball & James, 1987; Ball *et al.*, 1992). Their definition of Bravais lattices for bulk crystalline solids is given in Definition 1.

Definition 1 [adopted from Definition 2.1 in Ball et al. (1992)]. A set of points $\mathcal{L}$ in $\mathbb{R}^3$ is a Bravais lattice if and only if there exists an invertible matrix $\mathbf{E} \in \mathbb{R}^{3\times3}$ such that

$$\mathcal{L} = \mathcal{L}(\mathbf{E}) := \left\{\mathbf{x} : \mathbf{x} = \mathbf{E}\boldsymbol{\mu},\ \forall \boldsymbol{\mu} \in \mathbb{Z}^3\right\}. \quad (1)$$

The columns of $\mathbf{E}$ are three linearly independent vectors underlying the lattice basis while the components of the integer vector $\boldsymbol{\mu}$ are the contravariant components of a lattice vector written in the basis $\mathbf{E}$. Let $\mathbf{e}_1$, $\mathbf{e}_2$ and $\mathbf{e}_3$ be the three columns of $\mathbf{E}$; the calculation of a lattice vector is conducted as matrix multiplication:

$$\mathbf{x} = [\mathbf{e}_1\ \mathbf{e}_2\ \mathbf{e}_3]\begin{bmatrix}\mu^1\\ \mu^2\\ \mu^3\end{bmatrix} = \mathbf{e}_i\mu^i. \quad (2)$$

In the rightmost part of the equation above, the Einstein summation convention is used.

Definition 2. The unit cell of a Bravais lattice $\mathcal{L}(\mathbf{E})$ is

$$\mathcal{U} = \mathcal{U}(\mathbf{E}) := \left\{\mathbf{x} : \mathbf{x} = \mathbf{E}\mathbf{a},\ \forall \mathbf{a} \in [0, 1)^3\right\}. \quad (3)$$

The symmetry of a Bravais lattice $\mathcal{L}(\mathbf{E})$ is characterized by its point group.

Definition 3. A group of orthogonal transformations $\mathcal{R}$ is a point group of a Bravais lattice $\mathcal{L}(\mathbf{E})$ if and only if

$$\forall \mathbf{Q} \in \mathcal{R}, \mathbf{x} \in \mathcal{L} \rightarrow \mathbf{Q}\mathbf{x} \in \mathcal{L}. \quad (4)$$

It has been proven that (Ericksen, 1980; Pitteri, 1984; Ball *et al.*, 1992) an orthogonal transformation $\mathbf{Q}$ belongs to the point group of a Bravais lattice $\mathcal{L}(\mathbf{E})$ if and only if there exists a $\boldsymbol{\Lambda} \in GL(3, \mathbb{Z})$ such that

$$\mathbf{Q}\mathbf{E} = \mathbf{E}\boldsymbol{\Lambda}, \quad (5)$$

where $GL(3, \mathbb{Z})$ is the group of all 3×3 invertible integer matrices. Equation (5) is computed as

$$[\mathbf{Q}\mathbf{e}_1\ \mathbf{Q}\mathbf{e}_2\ \mathbf{Q}\mathbf{e}_3] = [\mathbf{e}_1\ \mathbf{e}_2\ \mathbf{e}_3]\begin{bmatrix}\lambda_1^1 & \lambda_2^1 & \lambda_3^1\\ \lambda_1^2 & \lambda_2^2 & \lambda_3^2\\ \lambda_1^3 & \lambda_2^3 & \lambda_3^3\end{bmatrix} \text{ for } \lambda_i^j \in \mathbb{Z}. \quad (6)$$

To consider the orientation invariance of the lattice parameters, we use the *lattice metric* tensor (Pitteri, 1998):

Definition 4. For a Bravais lattice $\mathcal{L}(\mathbf{E})$, the lattice metric tensor is

$$\mathbf{C} = \mathbf{E}^{\mathrm{T}}\mathbf{E}. \quad (7)$$

The matrix representation of a lattice metric tensor is always positive definite and symmetric. The lattice parameters of $\mathcal{L}(\mathbf{E})$ are a sextuplet $(p_1, p_2, p_3, p_4, p_5, p_6)$ depending on the lattice metric tensor through

Table 1
Lattice parameter sextuplets of the 14 Bravais lattices.

The column 'order of the point group' includes both proper and improper rotational symmetries.

	Bravais latttice	Lattice parameters	Order of the point group
1	Simple cubic (s.c.)	$a_0(1, 1, 1, 0, 0, 0)$	48
2	Face-centered cubic (f.c.c.)	$(\frac{a_0}{2^{1/2}}, \frac{a_0}{2^{1/2}}, \frac{a_0}{2^{1/2}}, \frac{1}{2}, \frac{1}{2}, \frac{1}{2})$	48
3	Body-centered cubic (b.c.c.)	$(\frac{3^{1/2}a_0}{2}, \frac{3^{1/2}a_0}{2}, \frac{3^{1/2}a_0}{2}, \frac{1}{3}, \frac{1}{3}, -\frac{1}{3})$	48
4	Hexagonal	$(a, a, c, 0, 0, \frac{1}{2})$	24
5	Trigonal	$(a, a, a, \cos\alpha, \cos\alpha, \cos\alpha)$	12
6	Tetragonal	$(a, a, c, 0, 0, 0)$	16
7	Body-centered tetragonal (b.c.t.)	$(\alpha, \alpha, \alpha, \frac{-2a^2+c^2}{4a^2}, \frac{c^2}{4a^2}, \frac{c^2}{4a^2})$†	16
8	Primitive orthorhombic (p.o.)	$(a, b, c, 0, 0, 0)$	8
9	Base-centered orthorhombic (b.c.o.)	$(\frac{\gamma}{2}, \frac{\gamma}{2}, c, 0, 0, \frac{-a^2+b^2}{\gamma^2})$‡	8
10	Face-centered orthorhombic (f.c.o.)	$(\frac{\gamma}{2}, \frac{\alpha}{2}, \frac{\beta}{2}, \frac{c^2}{\beta\alpha}, \frac{a^2}{\gamma\beta}, \frac{b^2}{\gamma\alpha})$‡	8
11	Body-centered orthorhombic (i.c.o.)	$(\frac{\alpha}{2}, \frac{\alpha}{2}, \frac{\alpha}{2}, \frac{\alpha^2-2b^2}{\alpha^2}, \frac{-\alpha^2+2c^2}{\alpha^2}, \frac{\alpha^2-2a^2}{\alpha^2})$§	8
12	Primitive monoclinic (p.m.)	$(a, b, c, 0, \cos\beta, 0)$	4
13	Base-centered monoclinic (b.c.m.)	$(\frac{m}{2}, \frac{m}{2}, c, -\frac{ac\cos\beta}{mc}, \frac{ac\cos\beta}{mc}, \frac{-a^2+b^2}{m^2})$¶	4
14	Triclinic	$(a, b, c, \cos\alpha, \cos\beta, \cos, \gamma)$	2

† $\alpha = (2a^2 + c^2)^{1/2}/2$. ‡ $\alpha = (b^2 + c^2)^{1/2}, \beta = (a^2 + c^2)^{1/2}, \gamma = (a^2 + b^2)^{1/2}$. § $\alpha = (a^2 + b^2 + c^2)^{1/2}$. ¶ $m = (a^2 + b^2)^{1/2}$.

$$p_1 = \left(C_1^1\right)^{1/2}, p_2 = \left(C_2^2\right)^{1/2}, p_3 = \left(C_3^3\right)^{1/2}, p_4 = \frac{C_2^3}{p_2p_3},$$
$$p_5 = \frac{C_3^1}{p_1p_3}, p_6 = \frac{C_1^2}{p_1p_2}. \quad (8)$$

The underlying periodicity of a Bravais lattice can be described by either the lattice metric tensor or the lattice parameters, which are both invariant under symmetry operations and rigid-body rotations. Table 1 lists the expressions of lattice parameters for all 14 Bravais lattices in 3D written in their primitive basis.

2.2. Multilattice and rebase

The basis $\mathbf{E}$ given in Definition 1 is also called the *primitive basis* of the Bravais lattice $\mathcal{L}(\mathbf{E})$, as there is only one point in its unit cell. However, crystallography theory often does not deal with the primitive lattice basis, because it is not always the most orthogonal basis for all types of Bravais lattices. To facilitate the crystallographic calculations, X-ray crystallographers usually use the *conventional basis* in their formula and equations. There are seven out of 14 Bravais lattices in Table 1: f.c.c., b.c.c., b.c.t., b.c.o., f.c.o., i.c.o. and b.c.m., whose primitive basis is different from their conventional basis. In these lattices, the unit cell $\mathcal{U}(\mathbf{K})$ where $\mathbf{K}$ is the conventional basis of the lattice consists of more than one lattice point of the original lattice $\mathcal{L}(\mathbf{E})$ inside. In fact the lattice spanned by the conventional basis $\mathbf{K}$ is a *sublattice* of the original Bravais lattice.

Definition 5. A sublattice of a Bravais lattice $\mathcal{L}(\mathbf{E})$ is a Bravais lattice formed by a subset of $\mathcal{L}(\mathbf{E})$.

By periodicity, if $\mathcal{L}(\mathbf{S})$ is a sublattice of $\mathcal{L}(\mathbf{E})$, $\mathbf{S}$ must be related to $\mathbf{E}$ via $\mathbf{S} = \mathbf{E}\mathbf{\Lambda}$ for some integer matrix $\mathbf{\Lambda}$. When $\det \mathbf{\Lambda} > 0$, the basis chirality is preserved. When $|\det \mathbf{\Lambda}| > 1$, $\mathcal{L}(\mathbf{E}\mathbf{\Lambda})$ is a Bravais lattice with fewer lattice points than $\mathcal{L}(\mathbf{E})$. The missing lattice points can be added back to the unit cell using a *multilattice* presentation defined as follows.

Definition 6. A set of points $\mathcal{M}$ is a multilattice if and only if there exist a basis $\mathbf{E}$ and a set of lattice points

$$\mathcal{W} = \left\{\mathbf{w}_i \in [0, 1)^3 : i = 1, \ldots, m\right\} \tag{9}$$

such that

$$\begin{aligned}\mathcal{M} &= \mathcal{M}(\mathbf{E}, \mathcal{W}) = \mathcal{L}(\mathbf{E}) + \mathbf{E}\mathcal{W} \\ &:= \left\{\mathbf{y} : \mathbf{y} = \mathbf{x} + \mathbf{E}\mathbf{w}, \forall \mathbf{x} \in \mathcal{L}(\mathbf{E}), \mathbf{w} \in \mathcal{W}\right\}.\end{aligned} \tag{10}$$

Such $\mathcal{M}$ is also called an m-lattice, due to $|\mathcal{W}| = m$.

By Definition 6, not every multilattice equals some Bravais lattice. A necessary condition for the multilattice $\mathcal{M}(\mathbf{S}, \mathcal{W})$ to be equivalent to a Bravais lattice is that $\mathbf{0} \in \mathcal{W}$. Any Bravais lattice $\mathcal{L}(\mathbf{E})$ equals a trivial 1-lattice $\mathcal{M}(\mathbf{E}, \{\mathbf{0}\})$, which should be equivalent to infinitely many multilattices by changing the basis (*i.e.* $\mathbf{S} = \mathbf{E}\mathbf{\Lambda}$ with $|\det \Lambda| = 1$) (Ball *et al.*, 1992). For those $\mathcal{M}(\mathbf{S}, \mathcal{W})$ where $\mathcal{L}(\mathbf{S} = \mathbf{E}\mathbf{\Lambda})$ is a sublattice of $\mathcal{L}(\mathbf{E})$, the number of lattice points within the unit cell $\mathcal{U}(\mathbf{S})$ equals $|\det \mathbf{\Lambda}|$. Physically, $|\mathcal{W}|$ represents the number of points in $\mathcal{M} \cap \mathcal{U}(\mathbf{S})$, which should be the quotient of the sizes of unit cells $\mathcal{U}(\mathbf{S})$ and $\mathcal{U}(\mathbf{E})$.

The symmetry of multilattices is described by space groups instead of point groups. Before defining space groups, we need to introduce the concept of isometry transformation.

Definition 7. An isometry transformation $(\mathbf{Q}|\mathbf{c})$ is a pair of an orthogonal transformation $\mathbf{Q} \in O(3)$ and a translation $\mathbf{c} \in \mathbb{R}^3$ that transforms any point $\mathbf{x} \in \mathbb{R}^3$ according to

$$(\mathbf{Q}|\mathbf{c})\mathbf{x} = \mathbf{Q}\mathbf{x} + \mathbf{c}. \tag{11}$$

Definition 8. A group of isometry transformations $\mathcal{G}$ is a *space group* of the multilattice $\mathcal{M}$ if and only if

$$\forall (\mathbf{Q}|\mathbf{c}) \in \mathcal{G}, \mathbf{x} \in \mathcal{M} \rightarrow \mathbf{Q}\mathbf{x} + \mathbf{c} \in \mathcal{M}. \tag{12}$$

If $\mathcal{M}(\mathbf{S}, \mathcal{W}) = \mathcal{L}(\mathbf{E})$, then the space group $\mathcal{G}$ of $\mathcal{M}$ is the same as the point group $\mathcal{R}$ of $\mathcal{L}$, that is

$$\mathcal{G} = \left\{(\mathbf{Q}|\mathbf{0}) : \forall \mathbf{Q} \in \mathcal{R}\right\}.$$

In crystallography, we use the multilattice to present each of the 14 Bravais lattices. Most frequently, we use the conventional multilattice for base-centered, face-centered and body-centered lattices. Let $\mathcal{M}(\mathbf{S} = \mathbf{E}\mathbf{\Lambda}, \mathcal{W})$ be the conventional multilattice of $\mathcal{L}(\mathbf{E})$; we use $\mathbf{X} = \mathbf{\Lambda}^{-1}$ as the *conversion matrix* that maps the coordinates written in terms of the primitive basis to the conventional basis. For example, we can choose the conventional basis $a_0\mathbf{I}$ to express the f.c.c. lattice using the multilattice

$$\mathcal{M}_{\text{f.c.c.}} = \mathcal{M}(a_0\mathbf{I}, \{\mathbf{w}_1, \mathbf{w}_2, \mathbf{w}_3, \mathbf{w}_4\}), \tag{13}$$

where

$$\mathbf{w}_1 = \begin{bmatrix}0\\0\\0\end{bmatrix}, \mathbf{w}_2 = \begin{bmatrix}\frac{1}{2}\\\frac{1}{2}\\0\end{bmatrix}, \mathbf{w}_3 = \begin{bmatrix}0\\\frac{1}{2}\\\frac{1}{2}\end{bmatrix}, \mathbf{w}_4 = \begin{bmatrix}\frac{1}{2}\\0\\\frac{1}{2}\end{bmatrix}. \tag{14}$$

The above 4-lattice $\mathcal{M}_{\text{f.c.c.}}$ is the same as $\mathcal{L}_{\text{f.c.c.}} = \mathcal{L}(\mathbf{E})$ with

$$\mathbf{E} = \frac{a_0}{2}\begin{bmatrix}1 & 0 & 1\\1 & 1 & 0\\0 & 1 & 1\end{bmatrix} \tag{15}$$

being the primitive lattice basis. The conversion matrix is

$$\mathbf{X} = \begin{bmatrix}\frac{1}{2} & 0 & \frac{1}{2}\\\frac{1}{2} & \frac{1}{2} & 0\\0 & \frac{1}{2} & \frac{1}{2}\end{bmatrix} = [\mathbf{w}_2\ \mathbf{w}_3\ \mathbf{w}_4]. \tag{16}$$

Let $\mathbf{x}$ be a point in $\mathcal{M}_{\text{f.c.c.}}$; we have

$$\mathbf{x} = a_0\mathbf{I}(\mathbf{n} + \mathbf{w}_i) \text{ for some } \mathbf{n} \in \mathbb{Z}^3 \text{ and } i \in \{1, 2, 3, 4\}. \tag{17}$$

That leads to

$$\mathbf{x} = \mathbf{E}\mathbf{X}^{-1}(\mathbf{n} + \mathbf{w}_i). \tag{18}$$

Since $\mathbf{X}^{-1}$ is an integer matrix and $\mathbf{X}^{-1}\mathbf{w}_i$ are integer vectors, by Definition 1 $\mathbf{x} \in \mathcal{L}(\mathbf{E})$. This proves that any point in $\mathcal{M}_{\text{f.c.c.}}$ is in $\mathcal{L}(\mathbf{E})$. Thus, $\mathcal{M}_{\text{f.c.c.}} = \mathcal{L}(\mathbf{E})$. Under the same coordinate system used in (13), the generators of $\mathcal{M}_{\text{f.c.c.}}$'s space group $Fm\bar{3}m$ (No. 225) can be represented as

$$\begin{aligned}&\left(\begin{bmatrix}1 & 0 & 0\\0 & 1 & 0\\0 & 0 & -1\end{bmatrix}\middle|\middle|\begin{bmatrix}0\\0\\0\end{bmatrix}\right),\\ &\left(\begin{bmatrix}0 & 0 & -1\\-1 & 0 & 0\\0 & -1 & 0\end{bmatrix}\middle|\middle|\begin{bmatrix}0\\0\\0\end{bmatrix}\right),\\ &\left(\begin{bmatrix}0 & -1 & 0\\-1 & 0 & 0\\0 & 0 & 1\end{bmatrix}\middle|\middle|\begin{bmatrix}0\\0\\0\end{bmatrix}\right).\end{aligned} \tag{19}$$

By direct calculation, (12) in Definition 8 can be verified.

Among the 14 Bravais lattices, there are seven choices of the conventional basis corresponding to the seven crystal systems. They are the bases of simple cubic, hexagonal, trigonal, primitive tetragonal, primitive orthorhombic, primitive monoclinic (with the b axis as the unique axis) and triclinic. The periodicity of the other non-primitive Bravais lattices can be expressed by the multilattice description using the corresponding conventional basis. Then each point in the sublattice $\mathcal{L}(\mathbf{E})$ in (10) is $\mathbf{x} = \mathbf{E}\boldsymbol{\mu}$ for some integer vector $\boldsymbol{\mu}$. Its components as an integer triplet (μ^1, μ^2, μ^3) are consistent with the notation of Miller indices for crystallographic direction introduced by William Hallowes Miller in crystallography (Miller, 1839). Since the reciprocal basis is derived by taking the inverse transpose of the conventional basis of the real

lattice, all the calculations for the reciprocal lattice remain the same as given in (10), except that the integer triplets represent the indices of crystallographic planes.

In order to represent the formation of a multilattice from a Bravais lattice with the conservation of all lattice points, we define the lattice operation *rebase* as follows.

Definition 9. Let the multilattice $\mathcal{M}(\mathbf{S}, \mathcal{W})$ be equal to the Bravais lattice $\mathcal{L}(\mathbf{E})$. An invertible matrix $\mathbf{L} \in \mathbb{R}^{3\times3}$ is a rebase of $\mathcal{M}$ if and only if there exists an integral matrix $\mathbf{\Lambda} \in \mathbb{Z}^{3\times3}$ such that

$$\mathbf{L} = \mathbf{S}^{-1}\mathbf{E}\mathbf{\Lambda}. \tag{20}$$

The rebased lattice $\mathcal{M}(\mathbf{S}', \mathcal{W}')$ is given by

$$\mathbf{S}' = \mathbf{E}\mathbf{\Lambda} \tag{21}$$

and

$$\mathcal{W}' = \mathbf{S}'^{-1}(\mathcal{L} \cap \mathcal{U}(\mathbf{S}')) := \left\{\mathbf{S}'^{-1}\mathbf{x} : \mathbf{x} \in \mathcal{L} \cap \mathcal{U}(\mathbf{S}')\right\}. \tag{22}$$

The rebased lattice of a Bravais lattice by Definition 9 does not change the symmetry. The following is an algorithm for the rebase operation using $\mathbf{S}'^{-1}(\mathcal{L} \cap \mathcal{U}(\mathbf{S}')) = \mathbf{S}'^{-1}\mathcal{L} \cap \mathcal{U}(\mathbf{I})$ and $\mathbf{S}'^{-1}\mathbf{E} = \mathbf{\Lambda}^{-1}$,

(i) Find the smallest eigenvalue λ of $\mathbf{\Lambda}^{-\mathrm{T}}\mathbf{\Lambda}^{-1}$. $\lambda > 0$ because $\mathbf{\Lambda}^{-\mathrm{T}}\mathbf{\Lambda}^{-1}$ is positive definite.

(ii) Find and locate all integer points in the cube $[-\lfloor 1/\lambda^{1/2}\rfloor, \lfloor 1/\lambda^{1/2}\rfloor]^3$.

(iii) For each of the integer points $\boldsymbol{\mu}$ visited in the previous step, the lattice point $\mathbf{w} \in \mathcal{W}'$ is computed as $\mathbf{w} = \mathbf{\Lambda}^{-1}\boldsymbol{\mu}$ if $\mathbf{w} \in [0, 1)^3$.

Continuing our example of the f.c.c. lattice, the matrix

$$\mathbf{L} = \begin{bmatrix} \frac{1}{2} & -\frac{1}{2} & 0 \\ \frac{1}{2} & \frac{1}{2} & 0 \\ 0 & 0 & 1 \end{bmatrix} \tag{23}$$

is a rebase matrix of $\mathcal{M}_{\text{f.c.c.}}$ because it is invertible and there is an integer matrix

$$\mathbf{\Lambda} = \begin{bmatrix} 1 & 0 & -1 \\ 0 & 1 & 1 \\ 0 & -1 & 1 \end{bmatrix} \tag{24}$$

such that $\mathbf{L} = (a_0\mathbf{I})^{-1}\mathbf{E}\mathbf{\Lambda}$. Since $\det\mathbf{\Lambda} = 2$, to make $\mathcal{M}(a_0\mathbf{L}, \mathcal{W})$ an equivalent representation of $\mathcal{M}_{\text{f.c.c.}}$ there should be two lattice points in $\mathcal{W}$. By (22), first we have

$$\mathcal{M}_{\text{f.c.c.}} \cap \mathcal{U}(a_0\mathbf{L}) = \left(\begin{bmatrix} 0 \\ 0 \\ 0 \end{bmatrix}, \begin{bmatrix} 0 \\ \frac{a_0}{2} \\ \frac{a_0}{2} \end{bmatrix}\right). \tag{25}$$

Then,

$$\mathcal{W} = \frac{\mathbf{L}^{-1}}{a_0}\left(\begin{bmatrix} 0 \\ 0 \\ 0 \end{bmatrix}, \begin{bmatrix} 0 \\ \frac{a_0}{2} \\ \frac{a_0}{2} \end{bmatrix}\right) = \left(\begin{bmatrix} 0 \\ 0 \\ 0 \end{bmatrix}, \begin{bmatrix} \frac{1}{2} \\ \frac{1}{2} \\ \frac{1}{2} \end{bmatrix}\right). \tag{26}$$

From the lattice metric tensor

$$a_0^2\mathbf{L}^{\mathrm{T}}\mathbf{L} = a_0^2\begin{bmatrix} \frac{1}{2} & 0 & 0 \\ 0 & \frac{1}{2} & 0 \\ 0 & 0 & 1 \end{bmatrix}, \tag{27}$$

the lattice parameters are $[a_0/(2)^{1/2}, a_0/(2)^{1/2}, a_0, 0, 0, 0]$. This set of lattice parameters together with the lattice points in (26) describe a body-centered tetragonal lattice. In this case, it in fact has a higher symmetry due to the special a/c ratio of $1/(2)^{1/2}$.

2.3. Crystal structure

To be consistent with the symmetry operations defined in the *International Tables for Crystallography*, we need to distinguish the two concepts: (i) lattice points and (ii) sites. A Bravais lattice, as well as the equivalent multilattices, defined above, describe only the lattice points. Only by attaching a motif of atoms to each lattice point can one get a *crystal structure*. Atomic positions in the motif are further divided into groups called sites, due to symmetry.

Definition 10. Let $\mathcal{M}(\mathbf{S}, \mathcal{W})$ be a multilattice that equals some Bravais lattice. A crystal structure made of a single atomic species with $\mathcal{M}$ as its underlying lattice is

$$\begin{aligned}\mathcal{S}(\mathcal{M}, \mathcal{Q}) = \mathcal{S}(\mathbf{S}, \mathcal{W}, \mathcal{Q}) &= \mathcal{M} + \mathbf{S}\mathcal{Q} \\ &:= \left\{\mathbf{x} : \mathbf{x} = \mathbf{m} + \mathbf{S}\mathbf{q}, \forall\mathbf{m} \in \mathcal{M}, \mathbf{q} \in \mathcal{Q}\right\},\end{aligned} \tag{28}$$

where the non-empty set

$$\mathcal{Q} = \left\{\mathbf{q}_\alpha \in [0, 1)^3 : \alpha = 1, \ldots, \nu\right\} \tag{29}$$

is the set of spatial positions occupied by atoms/molecules in the unit cell, which are usually referred to as atomic positions.

A crystal structure made of n atomic species with $\mathcal{M}$ is

$$\bigcup_{i=1}^{n}\mathcal{S}(\mathcal{M}, \mathcal{Q}_i), \tag{30}$$

where $\mathcal{S}(\mathcal{M}, \mathcal{Q}_i)$ is the structure for the ith species.

Applying a rebase matrix $\mathbf{L}$ as defined in Definition 9 to the underlying lattice of $\mathcal{S}(\mathbf{S}, \mathcal{W}, \mathcal{Q})$ leads to an equivalent structure $\mathcal{S}(\mathbf{S}', \mathcal{W}', \mathcal{Q}')$, where $\mathbf{S}' = \mathbf{S}\mathbf{L}$, $\mathcal{W}'$ is given by (22), and

$$\mathcal{Q}' = \mathbf{L}^{-1}\mathcal{Q} \bmod \mathbf{1}. \tag{31}$$

The 'mod $\mathbf{1}$' operation on a vector means adding or subtracting integers to move all of its components into $[0, 1)$. Equation (31) suggests $|\mathcal{Q}| = |\mathcal{Q}'|$ since $|\mathcal{W}||\mathcal{Q}| = |\det\mathbf{L}||\mathcal{W}'||\mathcal{Q}'|$ and $|\mathcal{W}| = |\det\mathbf{L}||\mathcal{W}'|$. In other words, we transform the underlying lattice according to (22), then attach the same motif to it using the new basis.

For example, we assign three atomic positions to the 4-lattice $\mathcal{M}_{\text{f.c.c.}}$ to construct a mono-species structure $\mathcal{S}(a_0\mathbf{I}, \{\mathbf{w}_1, \mathbf{w}_2, \mathbf{w}_3, \mathbf{w}_4\}, \mathcal{Q})$ where the set $\mathcal{Q}$ consists of

$$\mathbf{q}_1 = \left[\frac{1}{4}, \frac{1}{4}, \frac{1}{4}\right], \quad \mathbf{q}_2 = \left[\frac{1}{4}, \frac{1}{4}, \frac{3}{4}\right], \quad \mathbf{q}_3 = [0, 0, 0]. \tag{32}$$

We use the rebase matrix given in (23) to rewrite the structure $\mathcal{S}(a_0\mathbf{L}, \mathcal{W}', \mathcal{Q}')$. By equation (22), $\mathcal{W}'$ consists of two lattice points

$$\mathbf{w}'_1 = [0, 0, 0], \quad \mathbf{w}'_2 = \left[\frac{1}{2}, \frac{1}{2}, \frac{1}{2}\right], \tag{33}$$

and by equation (31) $\mathcal{Q}'$ consists of three atomic positions

$$\mathbf{q}'_1 = \left[\frac{1}{2}, 0, \frac{1}{4}\right], \quad \mathbf{q}'_2 = \left[\frac{1}{2}, 0, \frac{3}{4}\right], \quad \mathbf{q}'_3 = [0, 0, 0]. \tag{34}$$

This rebase changes the underlying lattice from four lattice points per unit cell to two, but keeps three atomic positions per unit cell.

Mathematically, a structure is also a multilattice:

$$\mathcal{S}(\mathbf{E}, \mathcal{W}, \mathcal{Q}) = \mathcal{M}(\mathbf{E}, (\mathcal{W} + \mathcal{Q}) \bmod \mathbf{1}).$$

Thus, $\mathcal{S}(\mathbf{E}, \mathcal{W}, \mathcal{Q})$ satisfies the same space group as $\mathcal{M}(\mathbf{E}, (\mathcal{W} + \mathcal{Q}) \bmod \mathbf{1})$. For a multi-species structure to satisfy a space group, all of its mono-species sub-structures must satisfy the same space group. The separation of $\mathcal{W}$ and $\mathcal{Q}$ in $\mathcal{S}(\mathbf{E}, \mathcal{W}, \mathcal{Q})$ is mainly by their physical meaning: the former are the lattice points, while the latter are the atomic positions. Atomic positions are often grouped into *sites*. Atoms in the same site must be positioned cooperatively to satisfy the space group of the structure.

Definition 11. A *site* of a structure $\mathcal{S}(\mathbf{E}, \mathcal{W}, \mathcal{Q})$ having the space group $\mathcal{G}$ is a subset of atomic positions, $\mathcal{A} \subseteq \mathcal{Q}$, such that $\mathcal{S}(\mathbf{E}, \mathcal{W}, \mathcal{A})$ still satisfies $\mathcal{G}$, but none of the proper subsets of $\mathcal{A}$ does.

We continue the above example of filling the 4-lattice $\mathcal{M}_{\text{f.c.c.}}$ in (13) using the $\mathbf{q}_1, \mathbf{q}_2, \mathbf{q}_3$ in (32). First, we directly verify that the structure satisfies the space group $Fm\bar{3}m$ generated by (19). Furthermore, by Definition 11 this structure occupies two sites:

$$\mathcal{A}_{8c} = \{\mathbf{q}_1, \mathbf{q}_2\}, \quad \mathcal{A}_{4a} = \{\mathbf{q}_3\}. \tag{35}$$

The *International Tables for Crystallography* list all 230 space groups in $\mathbb{R}^3$. The sites in Definition 11 are often classified as the *Wyckoff positions* (Aroyo *et al.*, 2006) among crystallographers and materials scientists. The subscripts 8*c* and 4*a* in (35) are examples of the common notations for Wyckoff positions. In X-ray experiments, the diffraction intensity strongly depends on the scattering of atoms occupying the certain sites of a crystal structure having special site symmetry, although the necessary condition of diffraction (*i.e.* Bragg condition) is governed by the underlying periodicity. X-ray analysis software generally requires the knowledge of both the lattice parameters for the skeleton lattice (*i.e.* parameters in Table 1), the target space group, and all sites occupied by different species of atoms.

For cubic structures, it is not very hard to make an *ansatz* for the sites in the conventional unit cell. For example, for most *AB*-type alloys, the site is among the special positions such as corners, side centers, face centers and body centers. In some cases, atoms of small radii occupy the tetrahedron interstitial sites such as $[\frac{1}{4}, \frac{1}{4}, \frac{1}{4}]$ and $[\frac{1}{4}, \frac{1}{4}, \frac{3}{4}]$. However, for some complex crystal structures with low symmetry, *e.g.* martensite structures, there is no reliable analytic way of obtaining the sites for each of the atoms. From the database of the binary phase diagram (Okamoto, 2010), we observe that many low-symmetry structures of metallic materials are in fact formed through solid–solid phase transformations from a high-temperature phase of cubic symmetry. Examples include steel, CuAl alloy, Nitinol, and many other Cu-based β shape memory alloys. Using the mathematical formulation of the crystal structure given in (28), we can derive the crystal structure of the low-symmetry phase from their cubic parent phase through the assigned lattice correspondences.

2.4. Lattice correspondences and orientation relationships

Consider a solid–solid phase transformation from the high-symmetry parent structure $\mathcal{S}_\text{A}$ to the low-symmetry product structure $\mathcal{S}_\text{M}$ of a specific atomic species. We assume the average lattice distortion that takes all atoms in $\mathcal{S}_\text{A}$ to the new equilibrium positions in $\mathcal{S}_\text{M}$ is a linear transformation $\mathbf{F} \in \mathbb{R}^{3\times3}$ that deforms a parent unit cell $\mathcal{U}_\text{A}$ – not necessarily a primitive or conventional one – to a product unit cell $\mathcal{U}_\text{M}$. Let $\mathbf{S}_\text{A}$ and $\mathbf{S}_\text{M}$ be the basis of the sublattices spanned by $\mathcal{U}_\text{A}$ and $\mathcal{U}_\text{M}$, respectively. In other words, the three column vectors of $\mathbf{S}_\text{M}$ and $\mathbf{S}_\text{A}$ are the three edges of $\mathcal{U}_\text{A}$ and $\mathcal{U}_\text{M}$, respectively. Then we have

$$\mathbf{S}_\text{M} = \mathbf{F}\mathbf{S}_\text{A}. \tag{36}$$

$\mathbf{S}_\text{M}$ and $\mathbf{S}_\text{A}$ are allowed to be freely rotated to any convenient orientation, because only the stretch part of $\mathbf{F}$ matters. As a convention, we usually pick $\mathbf{S}_\text{M}$ to be the conventional basis of the product structure. Then $\mathbf{S}_\text{A}$ must be chosen appropriately to have a 'similar size and shape' as $\mathbf{S}_\text{M}$. This results in that $\mathbf{S}_\text{A}$ is almost always different from the conventional basis $\mathbf{K}_\text{A}$ of the parent structure. The rebasis matrix expressed as

$$\mathbf{G} = \mathbf{K}_\text{A}^{-1}\mathbf{S}_\text{A} \tag{37}$$

transforms the conventional multilattice into the one with basis $\mathbf{S}_\text{A}$. Here we use the rebase matrix $\mathbf{G}$ to represent the *lattice correspondence* matrix for solid–solid phase transformation. That is, for any lattice point $\mathbf{x}$ in $\mathcal{L}(\mathbf{K}_\text{A})$, it can be expressed by its integer index $\boldsymbol{\mu}_k$ as $\mathbf{x} = \mathbf{K}_\text{A}\boldsymbol{\mu}_k$, which equals $\mathbf{S}_\text{A}\mathbf{G}^{-1}\boldsymbol{\mu}_k$ by (37). Therefore the index of the same vector $\mathbf{x}$ in basis $\mathbf{S}_\text{A}$ is

$$\boldsymbol{\mu}_s = \mathbf{G}^{-1}\boldsymbol{\mu}_k. \tag{38}$$

Note that $\boldsymbol{\mu}_s$ is not necessarily an integer index. During the phase transformation, the lattice correspondence matrix $\mathbf{G}$ asserts that the index $[\mu_k^1\mu_k^2\mu_k^3]$ in the parent phase becomes the index $[\mu_s^1\mu_s^2\mu_s^3]$ in the product phase, while the associated lattice points in parent and product phases are related through small distortions and rotations. Such an assertion underlies a parallelism between the parent and product phases. (Sometimes we can multiply $\boldsymbol{\mu}_s$ by an integer n to make it an integer triplet. This is possible because $\boldsymbol{\mu}_s$ is rational. Then $[n\mu_k^1\ n\mu_k^2\ n\mu_k^3]$ corresponds to $[\mu_s^1\mu_s^2\mu_s^3]$.)

Similarly for any lattice plane $\bar{\mathbf{x}} = \mathbf{K}_{\mathrm{A}}^{-\mathrm{T}}\bar{\boldsymbol{\mu}}_k$, there exists a corresponding index $\bar{\boldsymbol{\mu}}_s$ in basis $\mathbf{S}_{\mathrm{A}}^{-\mathrm{T}}$ calculated as

$$\bar{\boldsymbol{\mu}}_s = \mathbf{G}^{\mathrm{T}}\bar{\boldsymbol{\mu}}_k. \tag{39}$$

Then the index of the lattice plane $(\bar{\mu}_k^1\bar{\mu}_k^2\bar{\mu}_k^3)$ becomes the index of the plane $(\bar{\mu}_s^1\bar{\mu}_s^2\bar{\mu}_s^3)$ during the phase transformation.

In the literature, people use the *orientation relationship* as an alternative to the lattice correspondence. To derive an orientation relationship for a directional index $[\mu_k^1\mu_k^2\mu_k^3]_{\mathrm{A}}$ or a planar index $(\bar{\mu}_k^1\bar{\mu}_k^2\bar{\mu}_k^3)_{\mathrm{A}}$ written in the conventional basis of the parent phase, we calculate the corresponding $[\mu_s^1\mu_s^2\mu_s^3]_{\mathrm{M}}$ for direction and $(\bar{\mu}_s^1\bar{\mu}_s^2\bar{\mu}_s^3)_{\mathrm{M}}$ for plane by (38) and (39), and then express the orientation relationship as

$$[\mu_k^1\mu_k^2\mu_k^3]_{\mathrm{A}}||[\mu_s^1\mu_s^2\mu_s^3]_{\mathrm{M}};\quad (\bar{\mu}_k^1\bar{\mu}_k^2\bar{\mu}_k^3)_{\mathrm{A}}||(\bar{\mu}_s^1\bar{\mu}_s^2\bar{\mu}_s^3)_{\mathrm{M}}. \tag{40}$$

By (38), (39), (40) and the Cauchy–Born rule in (36), we generalize the presentation of orientation relationships and the associated transformation strains for solid–solid phase transformation through a unified quantity: the lattice correspondence matrix.

The linear transformation $\mathbf{F} = \mathbf{S}_{\mathrm{M}}\mathbf{S}_{\mathrm{A}}^{-1} \in \mathbb{R}^{3\times3}$ is considered as the deformation gradient underlying the symmetry-breaking phase transformation based on the Cauchy–Born hypothesis through a proper choice of lattice correspondences (Ericksen, 1980; Bhattacharya *et al.*, 2004; Cayron, 2019). To rationalize the lattice correspondences selection, it is shown (Chen, Song *et al.*, 2016; Koumatos & Muehlemann, 2016, 2017) that an admissible correspondences matrix should give the least transformation strain when used in (36), where the transformation strain is defined as $(\mathbf{F}^{\mathrm{T}}\mathbf{F} - \mathbf{I})^{1/2}$. The mathematical expressions of lattice correspondences vary from reference to reference. In this paper, we use the representation of the lattice correspondence matrix introduced by Chen, Song *et al.* (2016) consistent with the aforementioned assertions.

As an example, we assume the parent structure is $\mathcal{S}_{\mathrm{A}} = \mathcal{S}(\mathcal{M}_{\mathrm{f.c.c.}}, \{\mathbf{0}\})$. Consider the lattice correspondence matrix:

$$\mathbf{G} = \begin{bmatrix} \frac{1}{2} & 0 & -\frac{1}{2} \\ 0 & 1 & 0 \\ \frac{1}{2} & 0 & \frac{1}{2} \end{bmatrix}. \tag{41}$$

We can derive many orientation relationships by selecting different directional and planar indices of the parent phase. Among them, there are three typical directional and planar correspondences:

$$[100]_{\mathrm{A}}||[10\bar{1}]_{\mathrm{M}};\ (010)_{\mathrm{A}}||(010)_{\mathrm{M}}, \tag{42}$$

$$[\bar{1}10]_{\mathrm{A}}||[\bar{1}11]_{\mathrm{M}};\ (111)_{\mathrm{A}}||(110)_{\mathrm{M}}, \tag{43}$$

$$[\bar{1}01]_{\mathrm{A}}||[001]_{\mathrm{M}};\ (111)_{\mathrm{A}}||(110)_{\mathrm{M}}. \tag{44}$$

For b.c.c. product structure, the set of parallelisms in (42), (43) and (44) are the Bain (Bain, 1924), K–S (Kurdjumow & Sachs, 1935), N–W (Nishiyama, 1934; Schumann, 1974) orientation relationships in the γ–α transformation of steel often referred to in the literature. In fact they are essentially the same lattice correspondences.

2.5. Derived structure

The goal is to develop a technique, referred to as *derived structure* that helps the structure determination for the low-symmetry phase transformed from a high-symmetry phase through phase transformation.

This technique assumes the full crystallographic knowledge of the parent structure in the conventional basis $\mathbf{K}$, and some knowledge about the product phase that can help us to propose a lattice correspondence matrix $\mathbf{G}$. If a rough estimate of the lattice parameters is given, we can search for candidates of lattice correspondence matrices algorithmically (Chen, Song *et al.*, 2016).

Once a lattice correspondence matrix $\mathbf{G}$ is proposed, equations (22) and (31) calculate a *reference structure*

$$\mathcal{S}_{\mathrm{r}} = \mathcal{S}(\mathbf{S}_{\mathrm{r}} = \mathbf{KG}, \mathcal{W}_{\mathrm{r}}, \mathcal{Q}_{\mathrm{r}}). \tag{45}$$

The reference structure can not be used to index the diffraction pattern of the low-symmetry product phase, because it essentially represents the same structure $\mathcal{S}_{\mathrm{A}}$ of the parent phase by the rebase operation. Therefore it generates the same diffraction pattern as the parent phase. We need to distort the reference structure slightly to break its symmetry. First, we apply a small deformation $\mathbf{P}$ to the basis $\mathbf{S}_{\mathrm{r}}$. The generic form of $\mathbf{P}$ is

$$\mathbf{P} = \begin{bmatrix} \delta_1 & \gamma_{12} & \gamma_{13} \\ 0 & \delta_2 & \gamma_{23} \\ 0 & 0 & \delta_3 \end{bmatrix}, \tag{46}$$

where δ_1, δ_2, δ_3 are small stretches in the vicinity of 1, and γ_{12}, γ_{13}, γ_{23} are small shears in the vicinity of 0. This calculates a new basis $\mathbf{S}_{\mathrm{d}} = \mathbf{PS}_{\mathrm{r}}$. From the reference structure to the derived structure with basis $\mathbf{S}_{\mathrm{d}}$, both lattice points and sites may change to match the broken space-group symmetry of the distorted unit cell. The determination of the lattice points and sites is usually empirical. Without any pre-knowledge of the space group, we can always assign both to the '*P*1' description: $\{\mathbf{0}\}$ and $(\mathcal{W} + \mathcal{Q})$ mod $\mathbf{1}$, *i.e.* each of the atomic positions is a site with multiplicity 1. In the case we have some information on the space group, $\mathcal{W}_{\mathrm{r}}$ and $\mathcal{Q}_{\mathrm{r}}$ need to be redistributed and slightly shuffled to new sets of lattice points $\mathcal{W}_{\mathrm{d}}$ and atomic positions $\mathcal{Q}_{\mathrm{d}}$ with site symmetry included in the Wyckoff positions listed in the *International Tables for Crystallography* (Hahn *et al.*, 1983). The new *derived structure* is expressed as

$$\mathcal{S}_{\mathrm{d}} = \mathcal{S}(\mathbf{S}_{\mathrm{d}}, \mathcal{W}_{\mathrm{d}}, \mathcal{Q}_{\mathrm{d}}). \tag{47}$$

Note that the expression of $\mathcal{S}_{\mathrm{d}}$ may not be unique, which depends on the choices of the orientation and origin of the unit cell $\mathcal{U}(\mathbf{S}_{\mathrm{d}})$. The derived structure $\mathcal{S}_{\mathrm{d}}$ can be used to analyze and predict the low-symmetry phase such as indexing of the unknown diffraction pattern by XRD. If the result is not satisfactory, we iterate the above process to find another derived structure.

Using $\mathcal{S}_{\mathrm{A}} = \mathcal{S}(\mathcal{M}_{\mathrm{f.c.c.}}, \{\mathbf{0}\})$ as the parent structure and lattice correspondence (41) as an example, we can demonstrate the derived lattice by the following calculations. By rebase operation, the basis of reference structure is calculated as

$$\mathbf{S}_{\rm r} = a_0\mathbf{G} = a_0\begin{bmatrix} \frac{1}{2} & 0 & -\frac{1}{2} \\ 0 & 1 & 0 \\ \frac{1}{2} & 0 & \frac{1}{2} \end{bmatrix}. \quad (48)$$

According to (22), the collection of lattice points of the reference structure is

$$\mathcal{W}_{\rm r} = \mathbf{S}_{\rm r}^{-1}(\mathcal{M}_{\rm f.c.c.} \cup \mathcal{U}(\mathbf{S}_{\rm r})) = \left(\begin{bmatrix} 0 \\ 0 \\ 0 \end{bmatrix}, \begin{bmatrix} \frac{1}{2} \\ \frac{1}{2} \\ \frac{1}{2} \end{bmatrix}\right). \quad (49)$$

Our first attempt is to distort $\mathbf{S}_{\rm r}$ by $\delta_1 = \delta_3 = 0.9$, $\delta_2 = 1.05$, $\gamma_{12} = \gamma_{13} = \gamma_{23} = 0$ according to (46). The derived basis is

$$\mathbf{S}_{\rm d1} = a_0\begin{bmatrix} 0.45 & 0 & -0.45 \\ 0 & 1.05 & 0 \\ 0.45 & 0 & 0.45 \end{bmatrix}. \quad (50)$$

The lattice metric is then

$$\mathbf{S}_{\rm d1}^{\rm T}\mathbf{S}_{\rm d1} = a_0^2\begin{bmatrix} 0.6364 & 0 & 0 \\ 0 & 1.0500 & 0 \\ 0 & 0 & 0.6364 \end{bmatrix}, \quad (51)$$

which gives a tetragonal lattice ($0.6364a_0$, $1.05a_0$, $0.6364a_0$, 0, 0, 0). Together with $\mathcal{W}_{\rm r}$ in (49) and $\mathcal{Q}_{\rm r} = \{\mathbf{0}\}$, we have a body-centered tetragonal $I4/m$ (No. 877) with only the $2a$ site occupied.

Our second attempt is to further lower the unit-cell symmetry by an additional shear deformation $\gamma_{13} = -0.1$. Then the derived basis and the lattice metric are

$$\mathbf{S}_{\rm d2} = a_0\begin{bmatrix} 0.4 & 0 & -0.5 \\ 0 & 1.05 & 0 \\ 0.45 & 0 & 0.45 \end{bmatrix}, \quad (52)$$

$$\mathbf{S}_{\rm d2}^{\rm T}\mathbf{S}_{\rm d2} = a_0^2\begin{bmatrix} 0.3625 & 0 & 0.0025 \\ 0 & 1.0500 & 0 \\ 0.0025 & 0 & 0.4525 \end{bmatrix}. \quad (53)$$

The lattice parameters are ($0.6020a_0$, $1.05a_0$, $0.6727a_0$, 0, $\cos 89.65^\circ$, 0), which is a monoclinic lattice with the b axis as its unique axis. As its current form, it could be a Pm (No. 6) monoclinic with $1a$ and $1b$ sites occupied. That is $\mathcal{S}(\mathbf{S}_{\rm b2}, \{\mathbf{0}\}, \mathcal{W}_{\rm r})$, where $\mathcal{W}_{\rm r}$ is given by (49). But we could also shift the positions by $[\frac{1}{4}, \frac{1}{4}, \frac{1}{4}]$, which is equivalent to the isometry transformation $(\mathbf{I}|-\frac{1}{4}\mathbf{S}_{\rm b2}\mathbf{1})$, and get a new pair of lattice positions

$$\left(\begin{bmatrix} \frac{1}{4} \\ \frac{1}{4} \\ \frac{1}{4} \end{bmatrix}, \begin{bmatrix} \frac{3}{4} \\ \frac{3}{4} \\ \frac{3}{4} \end{bmatrix}\right). \quad (54)$$

By Definition 11 and the *International Tables for Crystallography*, this pair occupies a single site, $2e$, of the space group $P2_1/m$ (No. 11), with $x = z = \frac{1}{4}$. Finally we shuffle the site slightly to $x = 0.2$ and $z = 0.3$ and get the derived structure

$$\mathcal{S}_{\rm d2} = \mathcal{S}\left\{\mathbf{S}_{\rm d2}, \{\mathbf{0}\}, \left(\begin{bmatrix} 0.2 \\ 0.25 \\ 0.3 \end{bmatrix}, \begin{bmatrix} 0.8 \\ 0.75 \\ 0.7 \end{bmatrix}\right)\right\}. \quad (55)$$

If we have a reason to believe the monoclinic structure is m-layer modulated along the c axis, we conduct an extra rebase on $\mathcal{S}_{\rm d}$ by

$$\mathbf{M} = \begin{bmatrix} 1 & 0 & 0 \\ 0 & 1 & 0 \\ 0 & 0 & m \end{bmatrix}. \quad (56)$$

The new set of m lattice points $\mathcal{W}_m$ can be computed by (22) and the new two-atom motif $\mathcal{Q}_m$ is obtained by (31). We then redistribute $\mathcal{W}_m$ and $\mathcal{Q}_m$ into $\{\mathbf{0}\}$ and $(\mathcal{W}_m + \mathcal{Q}_m)$ mod $\mathbf{1}$. The result is a $P2_1/m$ structure with $2m$ atoms occupying m $2e$ sites. The overall lattice correspondence matrix is $\mathbf{MG}$. If needed, the symmetry of the derived structure can be further lowered by slight shuffles of each of the sites. For $m = 9$, the derived structure is considered as the M18R structure in the literature.

3. Structural determination of martensite CuAlMn

Among all shape memory alloys, CuAuZn, CuAlNi and CuAlZn alloy systems form the second largest group of material candidates used in research and development. However, their commercialization is highly confined due to the poor fatigue life when they are in a polycrystalline state. Compared with these Cu-based alloy systems, the CuAlMn system is much less developed. For some aluminium compositions, good ductility has been demonstrated in this alloy system (Sutou *et al.*, 2008). In-depth study of the crystallography and the formation of microstructure is greatly hindered in this system because of the lack of structural parameters for martensite. Some discussions about its micromechanical behaviors are based on the lattice parameters of the cubic-to-monoclinic transformation of its sibling system CuAlNi (Wang *et al.*, 2002; Fornell *et al.*, 2017). In this section, we will show how the derived lattice assists the analysis of the structural determination of the martensite structure of the CuAlMn alloy.

According to the binary phase diagram of the Cu–Al alloy system, the martensite can be induced by suppressing the eutectic transformation through a rapid cooling process. The high-temperature β phase directly transforms into an ordered structure β_1 (DO3 or $L2_1$) at $T_{\rm c}$ (marked as the red curve in Fig. 1). The β_1 phase further undergoes a martensitic transformation at temperature $M_{\rm s}$ marked as the blue curve in Fig. 1. This also works for ternary Cu-based β alloys doped by Mn (Sutou *et al.*, 1999), except that the β_1 zone (the yellow region in Fig. 1) and the composition-dependent $M_{\rm s}$ curve may vary with the addition of Mn. The symmetry of the product phase formed by martensitic transformation from the β_1 phase varies with the Al concentration (Warlimont & Delaey, 1974; Sutou *et al.*, 1999, 2002).

The most studied compositions of Cu–Al–Mn are those with Al compositions 14–17 at.% and Mn composition around 10 at.% (Kainuma *et al.*, 1996; Sutou *et al.*, 1999, 2002, 2004) since the alloys within this compositional range show a better ductility than CuAlNi and CuAlZn in polycrystalline form (Sutou *et al.*, 1999, 2008). The crystal structure of martensite has been characterized by both X-ray powder diffraction and

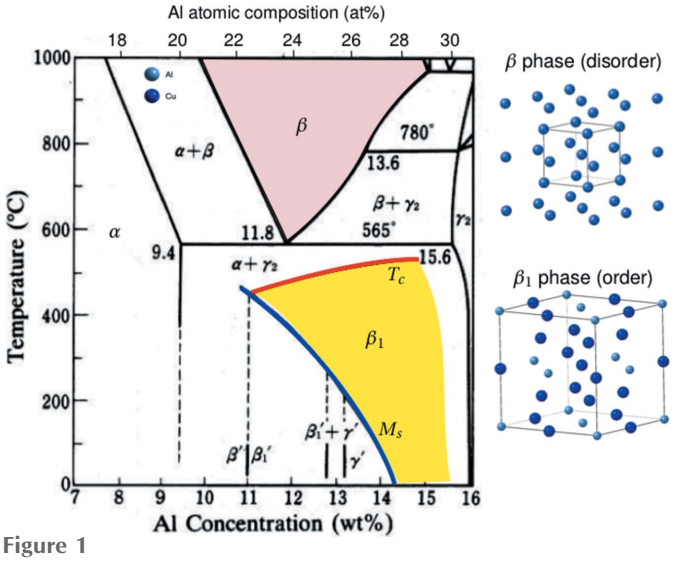

Figure 1
Binary phase diagram of Cu–Al alloy from Okamoto (2010).

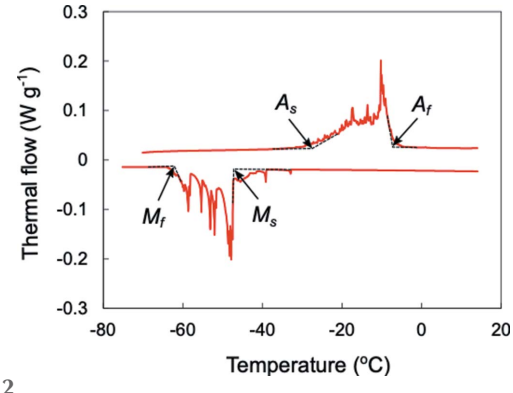

Figure 2
Differential scanning calorimetry of $CuAl_{24}Mn_9$.

transmission electron microscopy for Al compositions 14, 16 and 17 at.%. It was found that the martensite of as-aged samples is 18R (*i.e.* 18 layers modulated monoclinic structure). In our study, we choose the alloy of composition $Cu_{67}Al_{24}Mn_9$ (at.%) to demonstrate our derived structure theory; the understanding of martensitic structure for Al composition larger than 17 at.% has not been reported (Obradó *et al.*, 1997).

3.1. Experiment

A mixture of high-purity Cu (99.99 wt%), Al (99.999 wt%) and Mn (99.95 wt%) ingots was melted in a quartz tube placed in an evacuated (10^{-5} mbar; 1 mbar = 100 Pa) induction furnace under an argon atmosphere. The melt was injected into a cylindrical copper mold and solidified as a rod of diameter 5 mm. It was homogenized at 800°C for 3 h under an argon atmosphere, then cooled in the furnace. We cut the rod into thin slices of thickness 1 mm, which were sealed in a vacuum quartz tube, heat treated at 900°C for 1 h and quenched in water.

The transformation temperature of the specimen was measured by differential scanning calorimetry (DSC) by a TA Instruments Q1000 at a heating and cooling rate of 10°C min^{-1} for three complete thermal cycles in the range from −75°C to 20°C. The austenite start/finish A_s/A_f temperatures and martensite start/finish M_s/M_f temperatures are determined as the onsets of the heat absorption/emission peaks as shown in Fig. 2: $A_s = -26$°C, $A_f = -8$°C, $M_s = -48$°C and $M_f = -62$°C. The thermal hysteresis is quite large and measured to be $\Delta T = \frac{1}{2}(A_s + A_f - M_s - M_f) = 38$°C. Unlike those reported transforming Cu-based β alloys (Kainuma *et al.*, 1996; Mallik & Sampath, 2008), this one shows the thermal bursts in large magnitude over a wide temperature range during the phase transformation. Evidently this thermal signature was observed in a similar alloy system with slightly different mangenese compositions (Obradó *et al.*, 1997), but the detailed crystal structure of martensite has not been thoroughly studied for this series. In their work, the total entropy change from the cubic phase (austenite) is calculated based on the DSC measurements, which was found to be highly correlated to the average electron concentration (*i.e.* e/a) of the alloy. Only those with $e/a > 1.46$ showed the jerky thermal behaviors, which was conjectured to be a different type of martensitic transformation: b.c.c. to 2H. Their room-temperature powder diffraction measurement showed some residual peaks corresponding to the 2H structure. The martensite finish temperatures of this series are quite low, *i.e.* around −60°C; therefore room-temperature diffractometry with mixed phases is not sufficient to identify and solve the martensite crystal structure for the 2H phase, and the lattice parameters were not reported for this phase in any other CuAlMn system.

3.2. Advanced structural characterization by synchrotron X-ray microdiffraction

To obtain precise information for the crystal structures of austenite and martensite and to show how the derived structure theory assists the structure determination, we conducted a temperature-varying single-crystal synchrotron X-ray Laue microdiffraction experiment combined with monochromatic energy scans (Tamura, 2014) on beamline 12.3.2 of the Advanced Light Source, Lawrence Berkeley National Laboratory. The X-ray beam with energy bandpass from 6 to 24 keV was focused down to 1 µm in diameter by a pair of elliptically bent Kirkpatrick–Baez mirrors. The focused high-brightness X-rays illuminated a single grain of the bulk sample, and generated a single-crystal Laue pattern. We used the custom-made thermal stage (Chen, Tamura *et al.*, 2016) to drive the phase transformation of the bulk sample, which controls the sample temperature from −100°C to 200°C with a ramping rate of 15°C min^{-1}. The bulk sample was polished in the austenite form at room temperature. An optical microscope attached to the end-station optic box allows one to observe *in situ* the sample surface reliefs while collecting the Laue patterns at a specified sample position during the cooling process.

Figs. 3(*a*)–3(*c*) show the evolution of Laue patterns as the sample was cooled through the phase transformation temperature while the corresponding microstructures in Figs. 3(*d*)–3(*f*) sufficiently reveal that the Laue pattern in (*a*) purely represents the austenite phase. As the temperature decreased, we observed that martensite laths appear and grow as shown in Figs. 3(*e*) and 3(*f*). The Laue patterns (*b*) and (*c*) suggest that they are purely in the martensitic phase.

We used the $L2_1$ structure (space group $Fm\bar{3}m$) to index the austenite Laue pattern. The crystal structure is depicted in Fig. 4(*b*) (Tilley, 2006). The stoichiometric ratio of atoms for $L2_1$ is supposed to be ABC_2 where A atoms occupy the 4*a* site at $[0, 0, 0]$, B atoms occupy the 4*b* site at $[\frac{1}{2}, \frac{1}{2}, \frac{1}{2}]$ and C atoms occupy the 8*c* site at $[\frac{1}{4}, \frac{1}{4}, \frac{1}{4}]$. In the case of $Cu_{67}Al_{24}Mn_9$, we assume that the Al atoms occupy the 4*a* site, the Mn atoms occupy the 4*b* site and the Cu atoms occupy the 8*c* sites. Using the *XMAS* software (Tamura, 2014), we successfully indexed the Laue pattern by the proposed $L2_1$ structure as shown in Fig. 4(*a*). To determine the austenite lattice parameter, we chose four (*hkl*) reflections: (252), (170), (238) and (176), and precisely measured their interplanar distances by performing energy scans of the reflections. The refined lattice parameter was measured to be $a_0 = 5.87897$ Å.

In our notation the three mono-species sub-structures are

$$\mathcal{S}_i = \mathcal{S}(\mathcal{M}_{\text{f.c.c.}}, \mathcal{A}_i), i = \text{Al, Mn, Cu}, \tag{57}$$

where

$$\mathcal{A}_{\text{Al}} = \left(\begin{bmatrix}0\\0\\0\end{bmatrix}\right), \mathcal{A}_{\text{Mn}} = \left(\begin{bmatrix}\frac{1}{2}\\\frac{1}{2}\\\frac{1}{2}\end{bmatrix}\right), \mathcal{A}_{\text{Cu}} = \left(\begin{bmatrix}\frac{1}{4}\\\frac{1}{4}\\\frac{1}{4}\end{bmatrix}, \begin{bmatrix}\frac{1}{4}\\\frac{1}{4}\\\frac{3}{4}\end{bmatrix}\right). \tag{58}$$

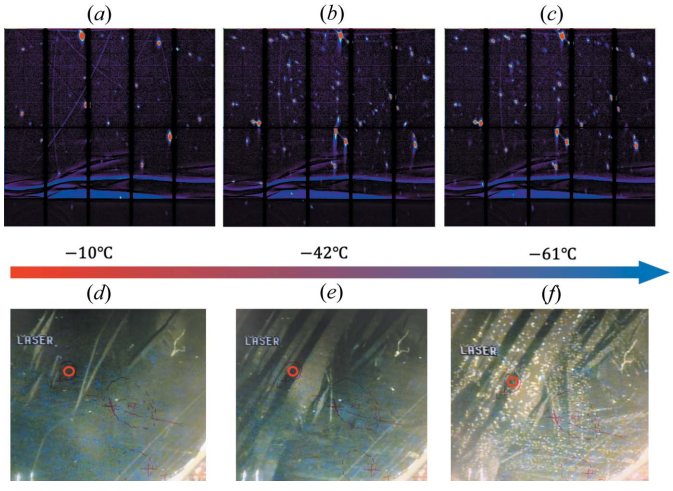

Figure 3
(*a*)–(*c*) Laue diffraction patterns of the bulk sample from high temperature to low temperature corresponding to the microstructures in (*d*)–(*f*), in which the red circles denote the surface positions illuminated by the focused X-ray beam.

3.3. Determination of martensitic structure by derived structure theory

We assume the Bain lattice correspondence for the phase transformation from $L2_1$ to orthorhombic:

$$\mathbf{G} = \begin{bmatrix}\frac{1}{2} & 0 & -\frac{1}{2}\\0 & 1 & 0\\\frac{1}{2} & 0 & \frac{1}{2}\end{bmatrix}. \tag{59}$$

As we have already shown in the examples in Section 2.5, the underlying multilattice is rewritten in the basis $a_0\mathbf{G}$ with lattice points in the set

$$\mathcal{W} = \left(\begin{bmatrix}0\\0\\0\end{bmatrix}, \begin{bmatrix}\frac{1}{2}\\\frac{1}{2}\\\frac{1}{2}\end{bmatrix}\right). \tag{60}$$

The new sets of atomic positions upon such basis transformation are, by (31),

$$\mathcal{Q}_{\text{Al}} = \left(\begin{bmatrix}0\\0\\0\end{bmatrix}\right), \mathcal{Q}_{\text{Mn}} = \left(\begin{bmatrix}0\\\frac{1}{2}\\0\end{bmatrix}\right), \mathcal{Q}_{\text{Cu}} = \left(\begin{bmatrix}\frac{1}{2}\\\frac{1}{4}\\0\end{bmatrix}, \begin{bmatrix}0\\\frac{1}{4}\\\frac{1}{2}\end{bmatrix}\right). \tag{61}$$

The new lattice parameters computed from $a_0^2\mathbf{G}^{\text{T}}\mathbf{G}$ are $[a_0/(2)^{1/2}, a_0, a_0/(2)^{1/2}, 0, 0, 0]$.

In Fig. 4(*d*), the red and blue boxes underlie the cells of $\mathcal{L}(a_0\mathbf{G})$. Our first attempt to generate a derived structure is to apply simple stretches $\delta_1 = 1.05$, $\delta_2 = 1.02$ and $\delta_3 = 0.92$ to $a_0\mathbf{G}$. The distorted lattice parameters are $(a_{\text{d}}, b_{\text{d}}, c_{\text{d}}, 0, 0, 0)$, where $a_{\text{d}} = 4.36491$, $b_{\text{d}} = 5.40865$ and $c_{\text{d}} = 4.2402$ Å. By observation, all three mono-species structures satisfy the

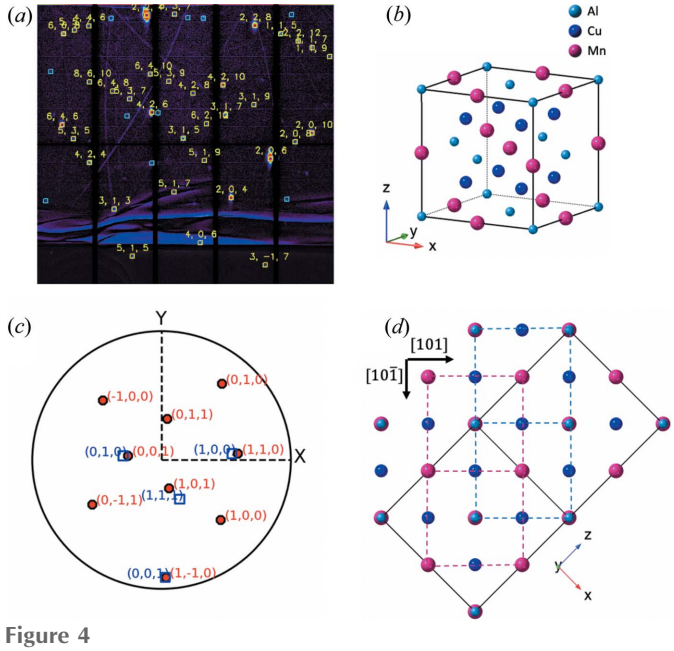

Figure 4
Austenite crystal structure of $Cu_{67}Al_{24}Mn_9$: (*a*) indexed Laue pattern by (*b*) the $L2_1$ structure. (*c*) The stereographic projection of the reciprocal lattices of austenite and the transformed martensite with respect to the stage coordinate system (*X*–*Y*–*Z*). (*d*) The theoretical atomic structure in the (010) plane that is aligned horizontally along the [101] direction.

Table 2
Wyckoff positions of derived *Immm* structure (Hahn *et al.*, 1983) for CuAlMn.

Atomic species	Wyckoff position	Site with lattice points: $[0,0,0]+[\frac{1}{2},\frac{1}{2},\frac{1}{2}]$
Al	2*a*	[0,0,0]
Mn	2*d*	$[\frac{1}{2},0,\frac{1}{2}]$
Cu	4*h*	$[0,y,\frac{1}{2}]$, $[0,\bar{y},\frac{1}{2}]$; $y=\frac{1}{4}$

Table 3
Wyckoff positions of derived *Pmmn* structure (Hahn *et al.*, 1983) for CuAlMn.

Atomic species	Wyckoff position	Site with lattice points: [0,0,0]
Al	2*a*	$[x,0,0]$, $[\bar{x},\frac{1}{2},\frac{1}{2}]$; $x=\frac{1}{3}$
Mn	2*b*	$[x,\frac{1}{2},0]$, $[\bar{x},0,\frac{1}{2}]$; $x=\frac{1}{3}$
Cu	4*e*	$[x,y,0]$, $[x,\bar{y},0]$, $[\bar{x},y+\frac{1}{2},\frac{1}{2}]$, $[\bar{x},\bar{y}+\frac{1}{2},\frac{1}{2}]$; $x=\frac{2}{3}$, $y=\frac{1}{4}$

Immm (No. 71) space group, with $\mathcal{Q}_{\rm Al}$, $\mathcal{Q}_{\rm Mn}$ and $\mathcal{Q}_{\rm Cu}$ being the 2*a*, 2*d* and 4*h* ($y=\frac{1}{4}$) sites, respectively (Table 2). We denote this new multi-species structure $\mathcal{S}_{Immm}$.

We use this crystal structure as input for the *XMAS* Laue indexing algorithm, and get the indexed Laue pattern of martensite. The indexing program suggests two martensite variants corresponding to the indexed reflections marked by yellow and orange colors, respectively, in Fig. 5(*c*). However, the indices of many major reflections are still not found by the crystal structure $\mathcal{S}_{Immm}$, which suggests the martensite may have a lower-symmetry structure.

Then we attempt to generate a second derived structure by further lowering its symmetry. First, we rewrite the $\mathcal{S}_{Immm}$ structure in the '*P*1' description. That means reducing the lattice point set {**0**}, and expanding the atomic positions to

$$\mathcal{Q}'_{\rm Al}=\left(\begin{bmatrix}0\\0\\0\end{bmatrix},\begin{bmatrix}\frac{1}{2}\\\frac{1}{2}\\\frac{1}{2}\end{bmatrix}\right),\ \mathcal{Q}'_{\rm Mn}=\left(\begin{bmatrix}0\\\frac{1}{2}\\0\end{bmatrix},\begin{bmatrix}\frac{1}{2}\\0\\\frac{1}{2}\end{bmatrix}\right),$$
$$\mathcal{Q}'_{\rm Cu}=\left(\begin{bmatrix}\frac{1}{2}\\\frac{1}{4}\\0\end{bmatrix},\begin{bmatrix}0\\\frac{1}{4}\\\frac{1}{2}\end{bmatrix},\begin{bmatrix}0\\\frac{3}{4}\\\frac{1}{2}\end{bmatrix},\begin{bmatrix}\frac{1}{2}\\\frac{3}{4}\\0\end{bmatrix}\right). \quad (62)$$

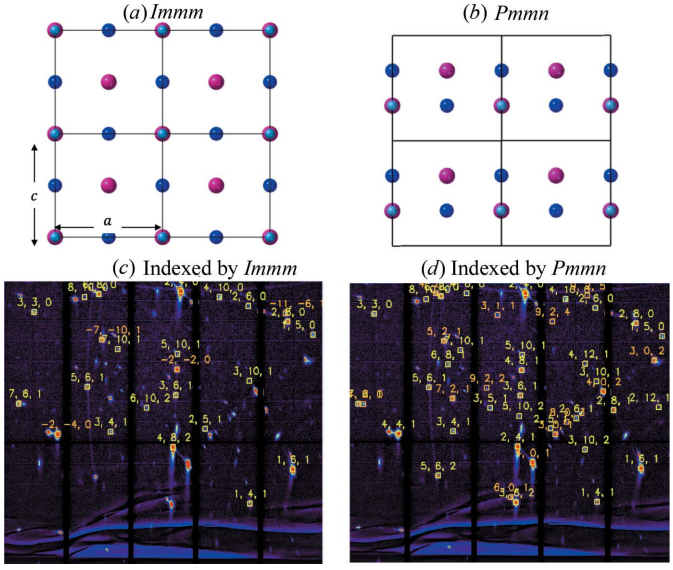

Figure 5
Derived orthorhombic structures of $CuAl_{24}Mn_9$ with space group (*a*) *Immm* and (*b*) *Pmmn*, by which the synchrotron X-ray Laue diffraction pattern of martensite is indexed in (*c*) and (*d*), respectively.

We then shift the origin to $[-\frac{1}{4},0,0]$, and get new atomic positions

$$\mathcal{Q}''_{\rm Al}=\left(\begin{bmatrix}\frac{1}{4}\\0\\0\end{bmatrix},\begin{bmatrix}\frac{3}{4}\\\frac{1}{2}\\\frac{1}{2}\end{bmatrix}\right),\ \mathcal{Q}''_{\rm Mn}=\left(\begin{bmatrix}\frac{1}{4}\\\frac{1}{2}\\0\end{bmatrix},\begin{bmatrix}\frac{3}{4}\\0\\\frac{1}{2}\end{bmatrix}\right),$$
$$\mathcal{Q}''_{\rm Cu}=\left(\begin{bmatrix}\frac{3}{4}\\\frac{1}{4}\\0\end{bmatrix},\begin{bmatrix}\frac{1}{4}\\\frac{1}{4}\\\frac{1}{2}\end{bmatrix},\begin{bmatrix}\frac{1}{4}\\\frac{3}{4}\\\frac{1}{2}\end{bmatrix},\begin{bmatrix}\frac{3}{4}\\\frac{3}{4}\\0\end{bmatrix}\right). \quad (63)$$

Now the structure satisfies the *Pmmn* (No. 59) space group (origin choice 1). (We change the special axis from *z* in the *International Tables for Crystallography* to *x*, which is crystallographically equivalent.) $\mathcal{Q}''_{\rm Al}$ occupies the 2*a* site with $x_{\rm Al}=\frac{1}{4}$, $\mathcal{Q}''_{\rm Mn}$ occupies the 2*b* site with $x_{\rm Mn}=\frac{1}{4}$ and $\mathcal{Q}''_{\rm Cu}$ occupies the 4*e* site with $x_{\rm Cu}=\frac{3}{4}$ and $y_{\rm Cu}=\frac{1}{4}$.

We then propose to shuffle $x_{\rm Al}$ and $x_{\rm Mn}$ to $\frac{1}{3}$, and $x_{\rm Cu}$ to $\frac{2}{3}$. In other words, the neighboring (012) planes move $a_{\rm d}/6$ along the *x* axis relative to each other, as frequently reported in Cu-based alloys (Warlimont & Delaey, 1974). Then we obtain the second derived structure $\mathcal{S}_{Pmmn}$ with atomic positions listed in (64) and Table 3:

$$\mathcal{Q}'''_{\rm Al}=\left(\begin{bmatrix}\frac{1}{3}\\0\\0\end{bmatrix},\begin{bmatrix}\frac{2}{3}\\\frac{1}{2}\\\frac{1}{2}\end{bmatrix}\right),\ \mathcal{Q}'''_{\rm Mn}=\left(\begin{bmatrix}\frac{1}{3}\\\frac{1}{2}\\0\end{bmatrix},\begin{bmatrix}\frac{2}{3}\\0\\\frac{1}{2}\end{bmatrix}\right),$$
$$\mathcal{Q}'''_{\rm Cu}=\left(\begin{bmatrix}\frac{2}{3}\\\frac{1}{4}\\0\end{bmatrix},\begin{bmatrix}\frac{1}{3}\\\frac{1}{4}\\\frac{1}{2}\end{bmatrix},\begin{bmatrix}\frac{1}{3}\\\frac{3}{4}\\\frac{1}{2}\end{bmatrix},\begin{bmatrix}\frac{2}{3}\\\frac{3}{4}\\0\end{bmatrix}\right). \quad (64)$$

Using the second derived crystal structure $\mathcal{S}_{Pmmn}$ as the input for the *XMAS* Laue indexing algorithm, we get the indexed Laue pattern of martensite in Fig. 5(*d*). All major reflections are indexed by two martensite variants, which implies that the possible crystal structure of martensite is likely to be $\mathcal{S}_{Pmmn}$.

Finally, the orientation relationship between the austenite ($Fm\bar{3}m$) and the derived martensite (*Pmmn*) is confirmed by overlapping their stereographic projections calculated from the indexed Laue patterns, shown in Fig. 4(*c*). The normal vectors of the crystallographic planes (001), ($1\bar{1}0$) and (110) in austenite lattice are parallel to those of the crystallographic planes (010), (001) and (100) in the lattice of one of the martensite variants. This result also confirms our conjecture of the lattice correspondence for the derived martensite structure by (59).

In the pure martensite phase, we conduct the monochromatic energy scan in a wide photon energy spectrum (*i.e.* from 8 to 16 keV), and the interplanar distance measures are listed in Table 4 for the indexed crystallographic planes in a reference Laue pattern. In general, the theoretical interplanar distance for a plane $\mathbf{h} = (hkl)$ can be expressed as $d_{\rm theo} = |\mathbf{E}^*\mathbf{h}|$ where $\mathbf{E}^* = \mathbf{E}^{-\rm T}$. Here $\mathbf{E}^*$ is the reciprocal-lattice basis for the Bravais lattice $\mathcal{L}(\mathbf{E})$. In the case of an orthorhombic lattice, the lattice basis $\mathbf{E}$ is a diagonal matrix with diagonal elements (a, b, c). The values of (a, b, c) are determined as the minimizers

$$(a^*, b^*, c^*) = \arg\min_{(a,b,c)\in\mathbb{R}^3} \sum_{\mathbf{h}\in\mathcal{H}} \|d_{\rm theo}(a, b, c; \mathbf{h}) - d_{\rm exp}(\mathbf{h})\|^2, \tag{65}$$

in which the set $\mathcal{H}$ consists of all selected $\mathbf{h} = (hkl)$ corresponding to the experimentally measured $d_{\rm exp}(\mathbf{h})$ listed in Table 4. We use the derived lattice parameters $(a_{\rm d}, b_{\rm d}, c_{\rm d})$ as the initial condition and get the refined lattice parameters a = 4.43196, b = 5.34533, c = 4.26307 Å. Using the refined lattice parameters, we calculated the interplanar distances for the (hkl) planes shown in Table 4, which agree with the measured values up to 0.01%.

Table 4
The results of the monochromatic energy scan and the corresponding indices obtained from numerical analysis for the martensite phase.

hkl	E (keV)	λ (Å)	2θ (°)	$d_{\rm exp}$ (Å)	$d_{\rm theo}$ (Å)	$d_{\rm exp}/d_{\rm theo}$
$(5\bar{4}\bar{1})$	11.0201	1.12507	101.1893	0.728038	0.727824	1.00029
$(6\bar{4}\bar{2})$	14.4006	0.860965	88.1896	0.618645	0.618648	1.00000
$(5\bar{4}\bar{2})$	13.4255	0.923498	82.8361	0.697982	0.697949	1.00005
$(4\bar{3}\bar{2})$	12.0003	1.033176	73.7746	0.860631	0.860778	0.99983
$(3\bar{2}\bar{2})$	11.3352	1.093798	59.2741	1.105955	1.105480	1.00043
$(5\bar{2}\bar{2})$	12.6406	0.980841	77.6421	0.782307	0.782578	0.99965
$(7\bar{2}\bar{1})$	13.1555	0.942451	101.2271	0.609698	0.609752	0.99991
$(5\bar{2}\bar{1})$	9.9452	1.246674	98.0783	0.825439	0.825409	1.00004
$(4\bar{1}\bar{2})$	12.0503	1.028889	64.3184	0.966504	0.966894	0.99960
$(60\bar{1})$	12.3899	1.000688	86.8573	0.727825	0.727816	1.00001
$(50\bar{1})$	10.7153	1.157076	83.5984	0.867996	0.867833	1.00019
$(40\bar{1})$	9.1151	1.360207	78.7222	1.072370	1.072365	1.00000

4. Conclusion

This paper provides a series of mathematical definitions for crystalline solids, which form the basis of a method to calculate the derived crystal structure for martensitic materials transformed from cubic austenite through solid–solid phase transformations. We classify the lattice points, atomic positions and sites, which are associated with the space-group symmetry in the *International Tables for Crystallography*. This approach is demonstrated in $Cu_{67}Al_{24}Mn_9$ alloy that undergoes a cubic-to-orthorhombic phase transformation. We derive two possible martensitic structures *Immm* and *Pmmn*, in which the derived structure *Pmmn* gives a promising indexing of the Laue pattern measured by synchrotron X-ray diffraction. It makes it possible to use the further monochromatic energy scan to refine the lattice parameters.

Funding information

MK and XC thank the HK Research Grants Council for financial support under grant Nos. 16207017 and 16201019. XC also thanks the Isaac Newton Institute for Mathematical Sciences for support and hospitality during the program 'The Mathematical Design of New Materials,' when work on this paper was undertaken. This work was supported by EPSRC grant No. EP/R014604/1. The research of YY is supported by City University of Hong Kong with the grant No. 9610391. Beamline 12.3.2 and the Advanced Light Source were supported by the Office of Science, Office of Basic Energy Sciences, of the US Department of Energy under Contract No. DE-AC02-05CH11231.

References

Aroyo, M. I., Perez-Mato, J. M., Capillas, C., Kroumova, E., Ivantchev, S., Madariaga, G., Kirov, A. & Wondratschek, H. (2006). *Z. Kristallogr. Cryst. Mater.* **221**, 15–27.
Bain, E. C. (1924). *Trans. AIME*, **70**, 25–47.
Ball, J. & James, R. (1987). *Arch. Ration. Mech. Anal.* **100**, 13–52.
Ball, J. M., James, R. D. & Smith, F. (1992). *Philos. Trans. R. Soc. London Ser. A*, **338**, 389–450.
Bhattacharya, K. *et al.* (2003). *Microstructure of Martensite: Why it Forms and How it Gives Rise to the Shape-Memory Effect*, Vol. 2. Oxford University Press.
Bhattacharya, K., Conti, S., Zanzotto, G. & Zimmer, J. (2004). *Nature*, **428**, 55–59.
Cayron, C. (2019). *Acta Cryst.* A**75**, 411–437.
Chang, L. & Read, T. (1951). *Trans. Met. Soc. AIME*, **191**, 47.
Chen, X., Cao, S., Ikeda, T., Srivastava, V., Snyder, G. J., Schryvers, D. & James, R. D. (2011). *Acta Mater.* **59**, 6124–6132.
Chen, X., Song, Y., Tamura, N. & James, R. D. (2016). *J. Mech. Phys. Solids*, **93**, 34–43.
Chen, X., Srivastava, V., Dabade, V. & James, R. D. (2013). *J. Mech. Phys. Solids*, **61**, 2566–2587.
Chen, X., Tamura, N., MacDowell, A. & James, R. D. (2016). *Appl. Phys. Lett.* **108**, 211902.
Chluba, C., Ge, W., Lima de Miranda, R., Strobel, J., Kienle, L., Quandt, E. & Wuttig, M. (2015). *Science*, **348**, 1004–1007.
Ericksen, J. (1980). *Arch. Ration. Mech. Anal.* **73**, 99–124.
Ericksen, J. (1991). *Mechanics and Thermodynamics of Continua*, pp. 145–158. Berlin, Heidelberg: Springer Verlag.
Ericksen, J. L. (2008). *Math. Mech. Solids*, **13**, 199–220.
Fornell, J., Tuncer, N. & Schuh, C. (2017). *J. Alloys Compd.* **693**, 1205–1213.
Hahn, T., Shmueli, U. & Arthur, J. W. (1983). *International Tables for Crystallography*, Vol. 1. Dordrecht: Reidel.
Kainuma, R., Takahashi, S. & Ishida, K. (1996). *Metall. Mater. Trans. A*, **27**, 2187–2195.
Koumatos, K. & Muehlemann, A. (2016). *Proc. R. Soc. London Ser. A*, **472**, 20150865.
Koumatos, K. & Muehlemann, A. (2017). *Acta Cryst.* A**73**, 115–123.
Kurdjumow, G. & Sachs, G. (1935). *Mitteilung aus dem Kaiser Wilhelm-Institut für Metallforschung*, p. 325.
Mallik, U. S. & Sampath, V. (2008). *Mater. Sci. Eng. A*, **481–482**, 680–683.
Miller, W. H. (1839). *A Treatise on Crystallography*. Cambridge: J. & J. J. Deighton.
Miyazaki, S., Ohmi, Y., Otsuka, K. & Suzuki, Y. (1982). *J. Phys. Colloq.* **43**, C4–255.
Nishiyama, Z. (1934). *Sci. Rep. Tohoku Univ.* **23**, 637.

Obradó, E., Mañosa, L. & Planes, A. (1997). *Phys. Rev. B*, **56**, 20–23.
Okamoto, H. (2010). *Desk Handbook: Phase Diagrams for Binary Alloys*, 2nd ed. Materials Park, Ohio: ASM International.
Otsuka, K. & Ren, X. (2005). *Prog. Mater. Sci.* **50**, 511–678.
Pitteri, M. (1984). *J. Elast.* **14**, 175–190.
Pitteri, M. (1998). *Int. J. Plast.* **14**, 139–157.
Schumann, H. (1974). *Krist. Techn.* **9**, 1141–1152.
Song, Y., Chen, X., Dabade, V., Shield, T. W. & James, R. D. (2013). *Nature*, **502**, 85–88.
Sutou, Y., Kainuma, R. & Ishida, K. (1999). *Mater. Sci. Eng. A*, **273–275**, 375–379.
Sutou, Y., Omori, T., Kainuma, R. & Ishida, K. (2008). *Mater. Sci. Technol.* **24**, 896–901.
Sutou, Y., Omori, T., Kainuma, R., Ishida, K. & Ono, N. (2002). *Metall. Mater. Trans. A*, **33**, 2817–2824.
Sutou, Y., Omori, T., Wang, J., Kainuma, R. & Ishida, K. (2004). *Mater. Sci. Eng. A*, **378**, 278–282.
Tadaki, T. (1998). *Shape Memory Materials*, pp. 97–116. Cambridge University Press.
Tamura, N. (2014). *XMAS: a Versatile Tool for Analyzing Synchrotron X-ray Microdiffraction Data.* London: Imperial College Press.
Tilley, R. (2006). *Crystals and Crystal Structures.* Chichester: John Wiley and Sons Inc.
Tolédano, P. & Dmitriev, V. (1996). *Reconstructive Phase Transitions in Crystals and Quasicrystals.* Singapore: World Scientific.
Wang, R., Gui, J., Chen, X. & Tan, S. (2002). *Acta Mater.* **50**, 1835–1847.
Warlimont, H. & Delaey, L. (1974). *Martensitic Transformations in Copper- Silver- and Gold-based Alloys*, Vol. 18. Oxford: Pergamon.
Weinan, E. & Ming, P. (2007). *Arch. Ration. Mech. Anal.* **183**, 241–297.
Young, R. A. (1993). *The Rietveld Method*. *IUCr Monographs on Crystallography*, Vol. 5. International Union of Crystallography/ Oxford Science Publications.